Multi-Physics Coupling Model for Thermal Hydraulics and Solute Transport in CRUD Deposits

Yan Liu[1], Xiaojing Liu[1(✉)], Sijia Du[2], Jiageng Wang[2], and Hui He[1]

[1] Shanghai Jiao Tong University, Shanghai, China
xiaojingliu@sjtu.edu.cn
[2] Nuclear Power Institute of China, Chengdu, Sichuan, China

Abstract. The porous Chalk River Unidentified Deposit (CRUD) depositions on the fuel cladding have a great impact on the heat transfer and power distribution of the reactor, resulting in a decrease in reactor safety and economy. In current paper, a multi-physics model is developed to simulate thermal hydraulics and boron hideout within the CRUD depositions. Processes including heat transfer, pressure drop, capillary flow, solute transport, chemical reactions and radiolysis reactions are fully coupled. The coolant flows through the capillary tubes in the porous medium and evaporates into steam at the surface of chimneys. The solute diffuses into the porous medium by capillary flow and maintains its chemical equilibrium. Chemistry and thermal hydraulics are coupled by saturation temperature that varies with solute concentrations. The new model can reasonably predict the distributions of temperature, pressure, Darcy velocity and chemical concentrations. This model shows the effect of evaporation at the chimney surface on CRUD temperature and boric acid concentration. In addition, the results show that boron hideout is caused by the accumulation of boric acid and the precipitation of $Li_2B_4O_7$ at the bottom of CRUD. The influence of morphology parameters such as porosity, thickness, and chimney geometry on heat transfer and solute transport within CRUD depositions is also evaluated.

Keywords: CURD · Boron hideout · Cips · Multi-Physics coupling

1 Introduction

The pressurized water reactor (PWR) core has been in a harsh environment of high temperature, high pressure and high radioactivity. The fuel performance of PWR core is a key factor affecting the safety and economy of the reactor. During the operation of nuclear reactors, the steam generator heat transfer tubes, the largest heat transfer area in the primary coolant circuit, are continuously scoured and eroded by the high-pressure subcooled coolant, producing a large number of oxidation corrosion products. Driven by subcooled boiling, metal ions and corrosion products in the primary coolant circuit deposit on the surface of the fuel cladding at the upper part of the reactor core, forming

a thin and porous scale layer, named as Chalk River Unidentified Deposit (CRUD) [1], shown in Fig. 1.

On the one hand, the thermal resistance of the fuel rods increases and the heat transfer deteriorates as a result of the deposition of corrosion products. On the other hand, the loose and porous CRUD depositions can strengthen local boiling, and the boric acid is continuously concentrated until precipitated and adsorbed by the depositions, resulting in the uneven distribution of boron in the axial direction of the fuel rods. Since ^{10}B has obvious neutron absorption capacity, the boron hideout within the CRUD depositions will distort the axial power distribution and cause the core power shift, known as CRUD-Induced Power Shift (CIPS) [2].

In order to evaluate the thermal hydraulics and solute transport within CRUD depositions, many previous studies [3–11] have developed a series of methods to simulate the heat and mass transfer in CRUD under PWR operating conditions, such as Boron-induced Offset Anomaly (BOA) [12] developed by EPRI and MAMBA-3D [13] developed by CASL. However, there are still relatively few studies on the impact of chimney boiling and morphology structure in CRUD.

In this paper, a thermal hydraulics and solute transport model is developed to realize the coupling of heat transfer, pressure drop, capillary flow, solute transport, chemical reactions and radiolysis reactions within the CRUD depositions. The influence of the evaporation at the chimneys surface on thermal hydraulics and solute transport is obtained. Additionally, the impact of CRUD morphology parameters such as porosity, thickness, chimney radius and chimney diameter is evaluated.
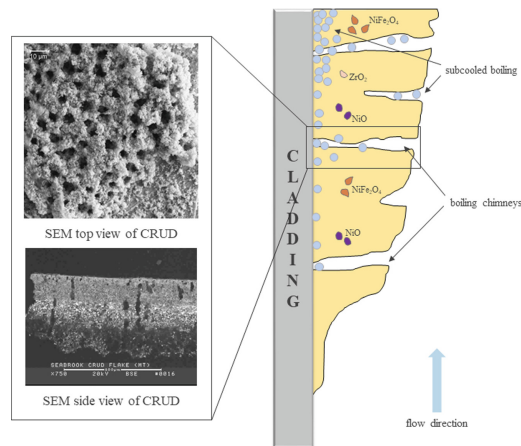

Fig. 1. The formation mechanism and microstructure schematic diagram of CRUD depositions

2 Model

The heat transfer, capillary flow, pressure drop, chemical reactions and radiolysis reactions within the CRUD depositions are tightly coupled. The coolant enters the capillary

tubes under the action of capillary force, evaporates into steam at the surface of the chimneys and escapes through the chimneys into the bulk coolant [7]. In this process, the solutes are concentrated and maintain the chemical equilibrium between other solutes, such as H_3BO_3, Li^+ and $B(OH)_4^-$. Boiling on the chimney surface enhances the concentration of solute, and the continuously concentrated solute in turn affects the saturation temperature of the coolant and chemical equilibrium between solutes within the CRUD depositions. In order to establish the multi-physics coupling model, a chimney and its surrounding porous structure (also called shell) are selected for research. The coordinates and boundary conditions are shown in Fig. 2.
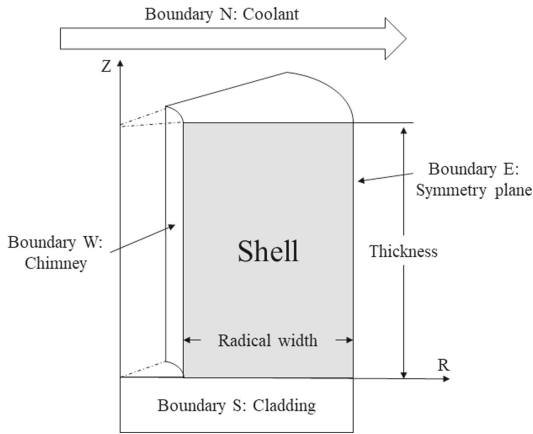
Fig. 2. Schematic diagram of coordinates and boundary conditions

2.1 Thermal Model

The coolant flows through the capillary tubes in the porous medium and evaporates into steam at the surface of chimneys. Based on the energy conservation, the governing equation of heat transfer within the CRUD depositions is derived as Eq. (1). Equations (2)–(5) represent the entrance of heat from cladding, its removal through the coolant interface, its removal through the chimney surface and its conduction on the symmetric plane, respectively.

$$\nabla(k_{CRUD}\nabla T) = 0 \tag{1}$$

$$-k_{CRUD}\left.\frac{\partial T}{\partial z}\right|_{z=0} = Q_{clad} \tag{2}$$

$$-k_{CRUD}\left.\frac{\partial T}{\partial z}\right|_{z=d} = h_c(T - T_f) \tag{3}$$

$$-k_{CRUD}\left.\frac{\partial T}{\partial r}\right|_{r=r_c} = -h_e(T - T_{sat}) \tag{4}$$

$$-k_{CRUD} \left. \frac{\partial T}{\partial r} \right|_{r=r_R} = 0 \tag{5}$$

where T is temperature; k_{CRUD} is the heat conductivity of the CRUD depositions; Q_{clad} is heat flux from the cladding surface; d is the CRUD thickness; h_c is conductive heat transfer coefficient at the CRUD and coolant interface, which usually takes the typical value 12000 W/(m × K) [9]; T_f is the bulk coolant temperature; r_c is chimney radius; h_e is conductive heat transfer coefficient at the chimney surface, which can be calculated as Eq. (6) suggested by Pan [8] et al.; T_{sat} is the saturation temperature, which is a function of solute concentration, and is usually described by the activity of water, a_w, which is also a function of solute concentration, shown as Eqs. (7)–(8) [14, 15]; r_R is the distance from the chimney center to the porous shell center (symmetric boundary), and it should be noted that the value is determined by the chimney density.

$$h_e = \left(\frac{2E}{2-E} \right) \left(\frac{M_{H_2O}}{2\pi R} \right)^{1/2} \frac{h_{fg}^2}{T^{3/2}(V_g - V_l)} \tag{6}$$

where E is the evaporation coefficient; M_{H2O} is the molecular weight of H_2O; R is the gas constant; h_{fg} is the vaporization enthalpy; V_g and V_l are the molecular volume of steam and water.

$$a_w = \frac{m_w}{m_w + \sum m_c} \tag{7}$$

$$
\begin{aligned}
T_{sat} = {} & 618.09 + 199.01(1 - a_w) - 952.74(1 - a_w)^2 \\
& + 26013.91(1 - a_w)^3 - 262916.0(1 - a_w)^4 \\
& + 997166.1(1 - a_w)^5
\end{aligned} \tag{8}
$$

where m_w is the mass molar concentration of water, equal to 55.509 mol/kg; m_c is the molar concentration of boric acid and other solutes.

2.2 Capillary Flow Model

The capillary flow with low fluid velocity within the porous CRUD depositions follows Darcy's low. The governing equation and boundary conditions are shown as Eqs. (9)–(13).

$$\nabla \cdot \left(-\varepsilon \rho_w \frac{\kappa}{\mu_w} \nabla P \right) = 0 \tag{9}$$

$$-\frac{\kappa}{\mu_w} \left. \frac{\partial P}{\partial z} \right|_{z=0} = 0 \tag{10}$$

$$P|_{z=d} = P_f \tag{11}$$

$$-\frac{\kappa}{\mu_w} \left. \frac{\partial P}{\partial r} \right|_{r=r_c} = -\frac{k_{CRUD}}{\rho_w h_{fg}} \frac{\partial T}{\partial r} \tag{12}$$

$$-\frac{\kappa}{\mu_w}\frac{\partial P}{\partial r}\bigg|_{r=r_R} = 0 \tag{13}$$

where P is pressure; ε is the porosity; ρ_w is the water density; κ is the permeability; μ_w is the water kinetic viscosity changing with temperature as Eq. (14) [16]; P_f is the pressure of bulk coolant.

$$\mu_w = \frac{25.3}{-8.58 \times 10^4 + 91 \cdot T + T^2} \tag{14}$$

In Darcy's law, the capillary flow velocity in the porous CRUD depositions is proportional to the pressure gradient as Eq. (15).

$$u_l = -\frac{\kappa}{\mu_w}\nabla P \tag{15}$$

where u_l, a vector with r and z directions, is the Darcy velocity of water within the CRUD depositions.

2.3 Solute Transport and Reaction Model

The governing equation of solute transport considers solute diffusion, convection, chemical reaction and radiolysis reaction, shown as Eq. (16). Due to the rapidity of reaction, solute transport and reaction within the CRUD depositions maintain in the quasi-steady state, so each item on the r.h.s of Eq. (16) can be considered zero. The boundary conditions are as Eqs. (17)–(20).

$$\frac{\partial C_i}{\partial t} = RC_i + RR_i - \nabla \cdot J_i \tag{16}$$

$$\frac{\partial C_i}{\partial z}\bigg|_{z=0} = 0 \tag{17}$$

$$C_i|_{z=d} = C_{f_i} \tag{18}$$

$$\left(-D_i\frac{\partial C_i}{\partial r} + u_{l_r}C_i\right)\bigg|_{r=r_c} = 0 \tag{19}$$

$$\frac{\partial C_i}{\partial r}\bigg|_{r=r_R} = 0 \tag{20}$$

where C is concentration; i represents the number of the solute; t is time; RC is the concentration changed by chemical reactions; RR is the concentration changed by radiolysis reactions; J is molar flux calculated as Eq. (21); D is diffusion coefficient, which is modified according to fractal theory as Eq. (22) [6].

$$J = -D\nabla C - DC\frac{zD\nabla\phi}{RT} + u_l C \tag{21}$$

$$D = \frac{\varepsilon}{\tau} D_w \tag{22}$$

where z is the solute's charge number; ϕ is the potential; τ is the tortuosity, which is a function of porosity as Eq. (23) [17]; D_w is the diffusion coefficient in pure water, and for boric acid, the value is 1.07×10^{-9} m^2/s in 298.15 K water, and at other temperatures the diffusion coefficient of boric acid satisfies the Stokes-Einstein relation [18] as Eq. (24).

$$\tau = \frac{1}{2} \left[1 + \frac{1}{2}\sqrt{1-\varepsilon} + \sqrt{1-\varepsilon} \frac{\sqrt{\left(\frac{1}{\sqrt{1-\varepsilon}} - 1\right)^2 + \frac{1}{4}}}{1 - \sqrt{1-\varepsilon}} \right] \tag{23}$$

$$D_w = 1.07 \times 10^{-9} \cdot \frac{T}{298.15} \cdot \frac{\mu_{w,T=298.15}}{\mu_w(T)} \tag{24}$$

The chemical reactions within the CRUD depositions considered include ionization of water, interactions of boric acid and water, and precipitation of boron. For a generalized chemical reaction as Eq. (25), the concentration changed by chemical reactions can be described as Eq. (26).

$$aA + bB \leftrightarrow cC + dD \tag{25}$$
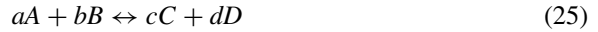
$$RC = -k_f C_A^a C_B^b + k_r C_C^c C_D^d \tag{26}$$

where uppercase letters represent participants in the chemical reaction and lowercase letters represent stoichiometric coefficients; k_f and k_r are forward and reverse reaction rate constants.

At equilibrium or quasi-steady state, $RC = 0$, so the ratio of the forward and reverse reaction rate constant is given by Eq. (27). The thermodynamic equilibrium expression[19] for the reaction is given by Eq. (28).
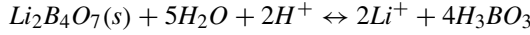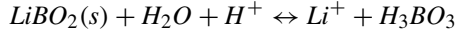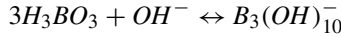
$$\frac{k_f}{k_r} = \frac{C_C^c C_D^d}{C_A^a C_B^b} \tag{27}$$

$$K = \frac{m_C^c m_D^d}{m_A^a m_B^b} \frac{\gamma_C^c \gamma_D^d}{\gamma_A^a \gamma_B^b} = \frac{k_f}{k_r} \frac{\gamma_C^c \gamma_D^d}{\gamma_A^a \gamma_B^b} (\zeta \rho_w)^{-a-b+c+d} \tag{28}$$

where K, the thermodynamic equilibrium expression, is a function of temperature corresponding to each chemical reaction; m is mass molar concentration; γ is the solute's activity coefficient; ζ is the correction of volume considering the solute volume.

The chemical reactions within the CRUD depositions considered in this paper include:

$$H_2O \leftrightarrow H^+ + OH^-$$

$$H_3BO_3 + OH^- \leftrightarrow B(OH)_4^-$$

$$2H_3BO_3 + OH^- \leftrightarrow B_2(OH)_7^-$$

$$3H_3BO_3 + OH^- \leftrightarrow B_3(OH)_{10}^-$$

$$LiBO_2(s) + H_2O + H^+ \leftrightarrow Li^+ + H_3BO_3$$

$$Li_2B_4O_7(s) + 5H_2O + 2H^+ \leftrightarrow 2Li^+ + 4H_3BO_3$$

The alpha dose within the CRUD depositions is raised by the concentrating boron via $^{10}B(n,\alpha)^7Li$ reaction. The solute concentration changed by radiolysis reactions can be considered as production RR_1, consumption and reproduction RR_2 two parts, which can be calculated by Eqs. (29) and (30) [20], respectively.

$$RR_1 = \left(\frac{G_\alpha \Gamma_\alpha + G_\alpha \Gamma_\alpha + G_\alpha \Gamma_\alpha}{100N_A} \right) f \rho_w \tag{29}$$

$$RR_2 = \sum \sum k_{AB} C_A C_B - C_C \sum k_D C_D \tag{30}$$

$$RR = RR_1 + RR_2 \tag{31}$$

where G is the number of molecules produced from the irradiation of 100 eV into a solution; Γ is dose rate; N_A is Avogadro's constant; f is a conversion factor from rad/sec to eV/(kg × sec); k is radiolysis reaction rate constant defined by Arrhenius law.

The radiolysis reactions within the CRUD depositions considered in this paper include:

$$H_2 + OH \leftrightarrow H + H_2O$$

$$H + H_2O_2 \leftrightarrow OH + H_2O$$
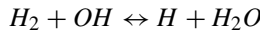
2.4 Numerical Approach and Coupling Scheme

The finite volume method is used to discrete in the two-dimensional cylindrical coordinates. The maximum relative error of temperature, pressure and solute concentration is used as the convergence condition, and the allowable maximum relative error is less than 10^{-7}. The thermal model, capillary flow model and solute transport and reaction model affect each other, and feedback each other in the coupling calculation process until the final calculation results converge. The whole calculation process is shown in Fig. 3.

The thermal model obtains temperature distribution and updates physical properties for capillary flow model and solute transport and reaction model. The pressure and Darcy velocity calculated by capillary flow model are used to determine the velocity of solute transport. The concentrations obtained by the solute diffusion and chemical reaction module update the saturation temperature, which has a significant influence on physical properties and then affects the temperature and pressure distribution.
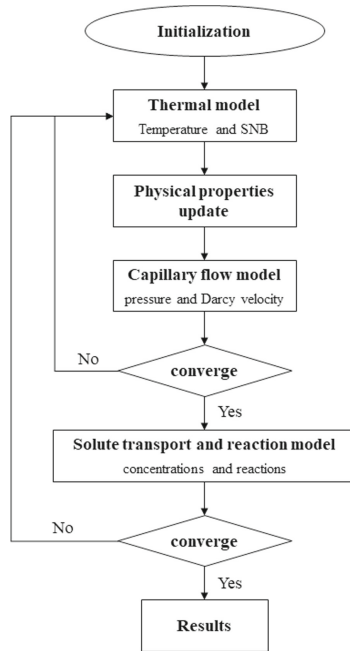
Fig. 3. Flow chart of the simulation process of CRUD heat and mass transfer

3   Results

In order to evaluate the thermal hydraulics and solute transport within the CRUD depositions, typical PWR thermal and hydrochemical conditions are selected for the analysis. Also the CRUD geometric parameters are chosen to evaluate the influence of CRUD morphology on the thermal hydraulics and solute transport. The overall input parameters are listed in Table 1.

Figure 4 shows the calculation results for the distributions of temperature, pressure, Darcy velocity, boric acid concentration, lithium concentration and pH within the CRUD depositions. The temperature reaches the maximum value of 642.42 K at the interface between the cladding and the symmetry plane. The maximum temperature difference is 26.53 K. The maximum subcooled boiling heat flux occurs at the interface between the cladding and the chimney, reaching 0.455 MW/m^2. At the same time, this region is also the position where the maximum pressure drop occurs reaching 2.8 kPa, making the capillary flow velocity of 0.78 mm/s in the R direction. The heat taken away by subcooled boiling at the chimney surface accounts for 61% of the total heat transfer through the CRUD depositions.

Table 1. Overall input parameters and analysis variables

Parameters	Units	Values	Variable quantity
System pressure	MPa	15.5	–
Coolant temperature	K	600	–
Heat flux	MW/m^2	1.50	–
Boric acid concentration	ppm	1200	–
Lithium concentration	ppm	2	–
Hydrogen concentration	cc(STP)/kg	25.3	–
Gamma dose rate	Mrad/h	1200	–
Neutron dose rate	Mrad/h	2400	–
Neutron flux	#/(cm^2 × s)	3.6×10^{14}	–
CRUD porosity	–	0.8	0.4, 0.5, 0.6, 0.7, 0.8
CRUD thickness	μm	60	20, 40, 60, 80
CRUD chimney radius	μm	2.5	1.5, 2.0, 2.5, 3.0
CRUD chimney density	$\times 10^3$/mm^2	3	1, 2, 3, 4

Boric acid concentration and lithium concentration are closely related to capillary flow within the CRUD depositions, which are affected by subcooled boiling at the chimney surface. The solutes reach the area near the chimney under the action of capillary flow. Since most of the solutes do not evaporate like water but get concentrated, so the concentrations in the area near the chimney are usually higher. At the interface between the cladding and the chimney, the boric acid concentration and lithium concentration reach the maximum values of 0.60 mol/L and 1.5 mmol/L, respectively. Although theoretically for chemical reactions, the more boric acid, the more reaction with OH-, due to the chemical equilibrium by temperature and other chemical reactions, even though the trend is roughly the same, the concentration ratio is different. Compared with the concentration in the bulk coolant, the maximum concentration ratios of $B(OH)_4^-$, $B_2(OH)_7^-$, $B_3(OH)_{10}^-$ are 4.04, 32.06 and 248.26, respectively. After H^+ enters the CRUD depositions with the coolant, its concentration decreases, because OH^- concentration increases accordingly to maintain the chemical equilibrium of boric acid and other boron elements. In the area near the interface between the chimney and the cladding, H^+ concentration increases because the reaction of boron precipitation produces H^+. As for boron precipitation, it is found that $Li_2B_4O_7$ always reaches the required concentration condition for precipitation before $LiBO_2$, so it is considered that boron is more inclined to precipitate in the form of $Li_2B_4O_7$.
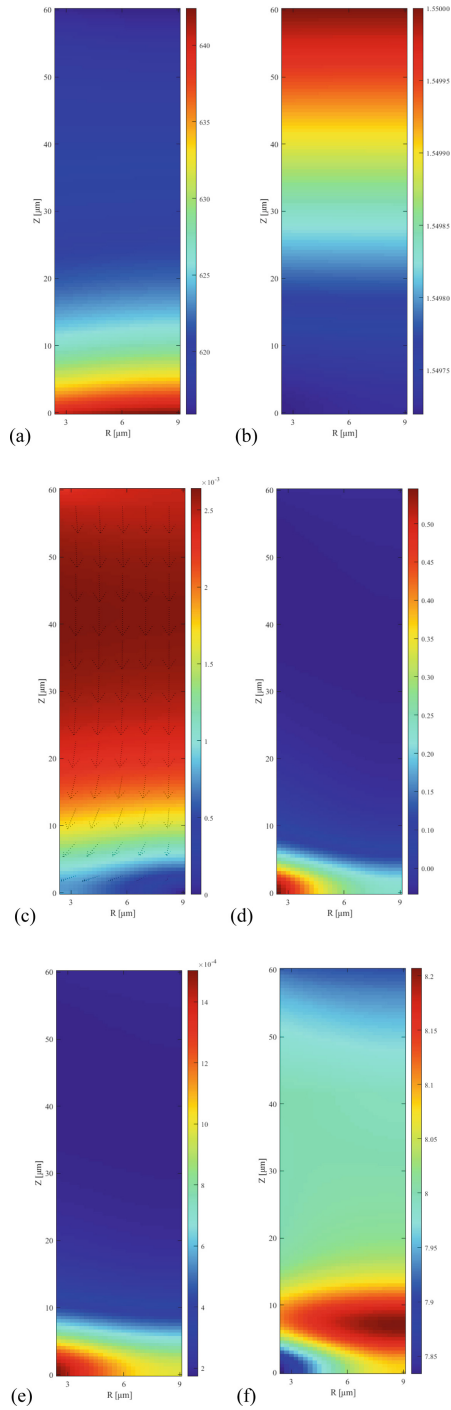
Fig. 4. The distributions of (a)temperature [K], (b)pressure [Pa], (c)Darcy velocity [m/s], (d)boric acid concentration [mol/L], (e)lithium concentration [mol/L], (f)pH within the CRUD depositions

4   Discussion

4.1   Influence of CRUD Porosity

Figure 5 plots the axial temperature difference, SNB heat removal ratio and boron mass through the CRUD depositions according to the CRUD porosity. Because the thermal conductivity of water is smaller than that of metal oxides constituting the CRUD porous structure, the higher the porosity is, the lower the CRUD thermal conductivity is, and the larger the temperature difference is. SNB heat removal ratio is approximately linear with the porosity, but the increase is not large. The diffusion coefficient corrected by fractal theory increase with the increase of the porosity. Because the capillary flow velocity is small and has little change, solutes with larger diffusion coefficients only need a smaller diffusion gradient to establish a balance with the convection. Therefore, the higher the porosity, the lower the solute concentration. But considering the volume fraction of coolant in the porous depositions, boron mass increases with the increase of porosity. The boron mass per unit area of CRUD is obtained by multiplying the boron mass of a chimney-centered calculation area by the chimney density.
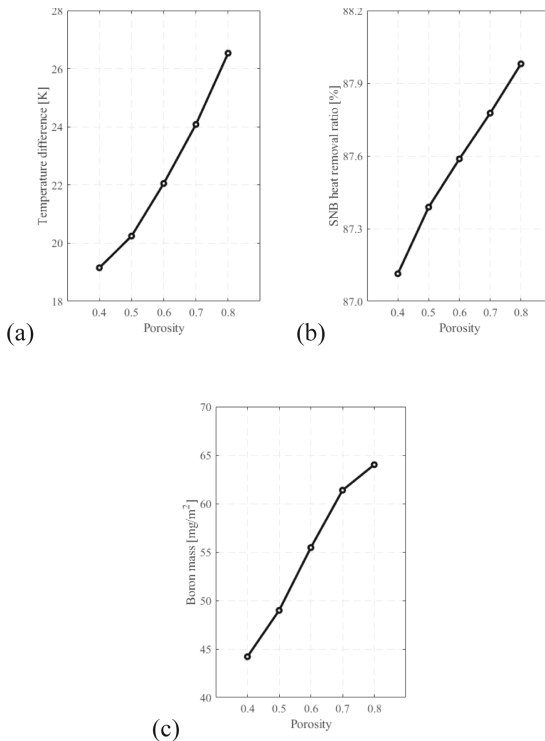
Fig. 5. (a) Axial temperature difference at the chimney surface, (b) SNB surface heat removal ratio, (c) boron mass per square meter CRUD along with the CRUD porosity
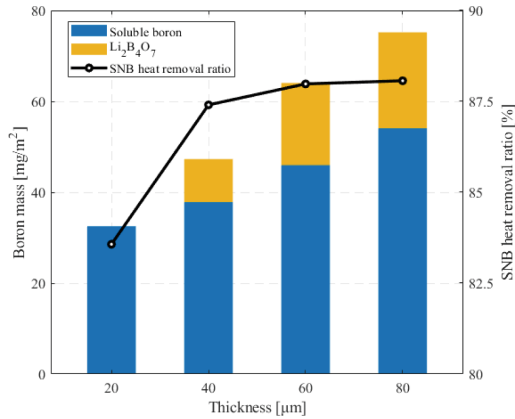
4.2 Influence of CRUD Thickness

Fig. 6. Boron hideout and SNB heat removal ratio along with the CRUD thickness

Figure 6 shows the boron hideout and SNB heat removal ratio within the CRUD depositions according to the CRUD thickness. With the increase of CRUD thickness, boron is also accumulated and the mass increases. $Li_2B_4O_7$ has been precipitated a lot when the CRUD thickness reaches 40 μm, which is quite different from the characteristics reported by EPRI [2] that precipitation $LiBO_2$ begins to precipitate between 35–42 μm CRUD thickness. This also indicates that $Li_2B_4O_7$ reaches the precipitation condition earlier than $LiBO_2$. After the beginning of boron precipitation, the increasing trend of soluble boron mass slows down, and more boron is precipitated in the form of precipitation $Li_2B_4O_7$. At the same time, SNB heat removal ratio increases slightly after the thickness reaches 40 μm.

## 4.3 Influence of CRUD Chimney Radius

Figure 7 plots the axial temperature difference, pressure drop maximum and boric acid concentration maximum through the CRUD depositions according to the CRUD chimney radius. For a certain chimney density, the increase of chimney radius means the decrease of the shell area and the increase of the phase change area at the surface of the chimney. Therefore, with the increase of the chimney radius, more subcooled boiling occurs at the surface of the chimney, and less heat is removed by heat conduction, leading to smaller temperature difference and greater pressure drop. But larger chimney radius also means that the solutes are easier to reach the surface of the chimney and more difficult to diffuse to the interface between the cladding and the CRUD, and the maximum boric acid concentration decreases accordingly.

(a)   (b)   (c)
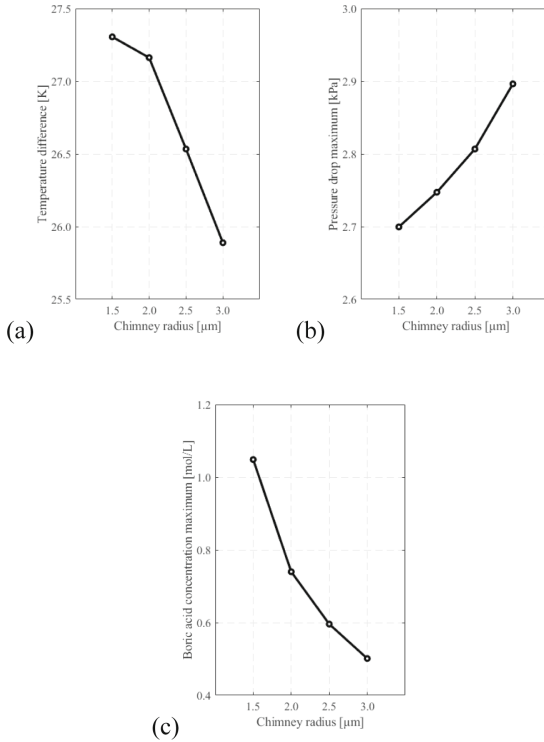
Fig. 7. (a) Axial temperature difference at the chimney surface, (b) pressure drop maximum, (c) boric acid concentration maximum along with the CRUD chimney radius

4.4 Influence of CRUD Chimney Density

Figure 8 plots the axial temperature difference, pressure drop maximum and boric acid concentration maximum through the CRUD depositions according to the CRUD chimney density. Similar to the effect of increasing the chimney radius, the increased chimney density also squeezes the area share of the CRUD porous shell and reduces the radial length (the distance from the chimney surface to the symmetric plane). Therefore, with the increase of chimney density, the temperature difference decreases, the pressure drop increases, and the maximum concentration of boric acid decreases.
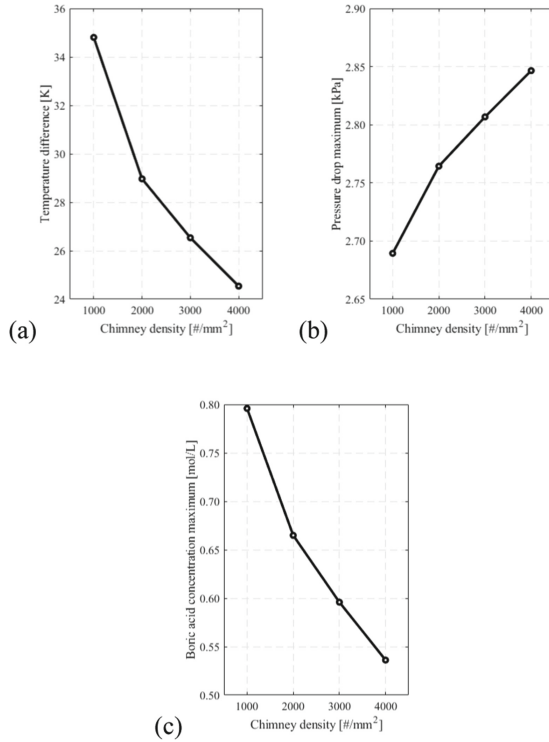
Fig. 8. (a) Axial temperature difference at the chimney surface, (b) pressure drop maximum, (c) boric acid concentration maximum along with the CRUD chimney density

5 Conclusion

The multi-physics coupling model is developed to predict the thermal hydraulics and solute transport within the porous CRUD depositions. Processes including heat transfer, pressure drop, capillary flow, solute transport, chemical reactions and radiolysis reactions are fully coupled. This model reasonably predicts the distributions of the temperature, pressure, Darcy velocity and solute concentrations within the CRUD depositions. The subcooled boiling at the surface of the chimney has an important influence on the thermal hydraulics and solute transport within the CRUD depositions. Temperature, pressure, SNB heat removal ratio, solute concentrations and boron mass are evaluated under different CRUD morphology parameters. With the increase of thickness, more boron exists in the form of precipitated $Li_2B_4O_7$. The porosity, chimney radius and chimney density have positive correlations with subcooled boiling and negative correlation with boron concentration. The thermal hydraulics and solute transport analysis by this model can provide technical support for the prediction of the CIPS phenomenon.

References

1. Li, S., Liu, X.: Development of boron tracking and boron hideout (CRUD) model based on subchannel approach. Nucl. Eng. Des. **338**, 166–175 (2018)
2. Deshon, J.: PWR axial offset anomaly (AOA) guidelines, revision 1," EPRI, Palo Alto, CA, 1008102(3) (2004)
3. Jaiswal, A.: A numerical study on parameters affecting boric acid transport and chemistry within fuel corrosion deposits during crud induced power shift (2013)
4. Park, B.G., Seo, S., Kim, S.J., Kim, J.H., Choi, S.: Meso-scale multi-physics full coupling within porous CRUD deposits on nuclear fuel. J. Nucl. Mater. **512**, 100–117 (2018)
5. Pan, C., Jones, B.G., Machiels, A.J.: Concentration levels of solutes in porous deposits with chimneys under wick boiling conditions. Nucl. Eng. Des. **99**, 317–327 (1987)
6. Short, M., Hussey, D., Kendrick, B., Besmann, T., Stanek, C., Yip, S.: Multiphysics modeling of porous CRUD deposits in nuclear reactors. J. Nucl. Mater. **443**(1–3), 579–587 (2013)
7. Macbeth, R.: Boiling on surfaces overlayed with a porous deposit: heat transfer rates obtainable by capillary action. Atomic Energy Establishment, Winfrith (England) (1971)
8. Pan, C., Jones, B., Machiels, A.: Wick boiling performance in porous deposits with chimneys. In: Proceedings of 23rd National Heat Transfer Conference, American Society of Mechanical Engineers (ASME), pp. 15–24
9. Haq, U.: Heat and mass transfer analysis for crud coated PWR fuel. Imperial College London (2011)
10. Zou, L., Zhang, H., Gehin, J., Kochunas, B.: A coupled TH/Neutronics/CRUD framework in prediction of cips phenomenon, Idaho National Lab.(INL), Idaho Falls, ID (United States) (2012)
11. Cohen, P.: Heat and mass transfer for boiling in porous deposits with chimneys
12. Deshon, J., Hussey, D., Kendrick, B., McGurk, J., Secker, J., Short, M.: Pressurized water reactor fuel crud and corrosion modeling. JoM **63**(8), 64–72 (2011)
13. Kendrick, B., Petrov, V., Walker, D., Manera, A.: CILC studies with comparative analysis to existing plants," CASL-U-2013–0224–000, Los Alamos National Laboratory (2013)
14. Pitzer, K., Brewer, L.: Thermodynamics. International Student Edition. McGraw-Hill, New York, NY (1961)
15. Deshon, J.: Modeling PWR fuel corrosion product deposition and growth processes, EPRI, Palo Alto, CA, 1009734 (2004)
16. Gierszowski, P., Mikic, B., Todreas, N.: Property correlations for lithium, sodium, helium, flibe and water in fusion reactor applications (1980)
17. Yu, B., Li, J.: Some fractal characters of porous media. Fractals **9**(03), 365–372 (2001)
18. Cappelezzo, M., Capellari, C., Pezzin, S., Coelho, L.: Stokes-Einstein relation for pure simple fluids. J. Chem. Phys. **126**(22), 224516 (2007)
19. Marshall, W.L., Franck, E.: Ion product of water substance, 0–1000°C, 1–10,000 bars New International Formulation and its background. J. Phys. Chem. Ref. Data **10**(2), 295–304 (1981)
20. Christensen, H.: Fundamental aspects of water coolant radiolysis, Swedish Nuclear Power Inspectorate (2006)